Bridging Structural and Dynamical Models of a Confined Sodium Nitroprusside Complex

Fabien Deligey, Sabine Bouguet-Bonnet, Abdelatif Doudouh, Pierre-Louis Marande, Dominik Schaniel, Axel Gansmuller

Bridging Structural and Dynamical Models of a Confined Sodium Nitroprusside Complex

*Fabien Deligey, Sabine Bouguet-Bonnet, Abdelatif Doudouh, Pierre-Louis Marande, Dominik Schaniel, Axel Gansmüller**

Université de Lorraine, CNRS, CRM2, F-54000 Nancy, France

E-mail :axel.gansmüller@univ-lorraine.fr

Phone : +33 (0)3 72 74 52 58

ABSTRACT

Sodium nitroprusside (SNP), an active pharmaceutical ingredient, is encapsulated in biocompatible amorphous silica matrices and characterized by Solid-State NMR. We previously showed by complementary NMR and Pair Distribution Function (PDF) study, that when confined in 1-2nm sized nanopores of an amorphous silica matrix, the complex displays "liquid like" isotropic motion (NMR) but still retains an associated anion/cation preferential arrangement (PDF). In this study we present new insights on the physical state of the confined drug, in order to explain the coexistence of these two seemingly contradictory characteristics. By performing temperature-dependent T_1 relaxation experiments on samples with different hydration levels, we retrieve respective motional activation energies for all three guest species inside the pores (Sodium cations, nitroprusside anions and water). For the hydrated samples we identify a temperature range where results ascertain isotropic but correlated ionic motion of the SNP ions. Contrastively, for the driest samples we detect NMR interactions that unravel adsorbed guest populations interacting with the pore surface. These descriptions of SNP dynamical properties clarify its unusually high ability to crystallize inside mesoporous matrices.

1) Introduction

Sodium nitroprusside (SNP) is a water-soluble salt, which is used in clinical practice as an efficient way to release NO[1,2]. Indeed, being an arterial and venous vasodilator, SNP has numerous applications in surgery and in response to heart failures, thanks to its ability to lower blood pressure[3]. However, SNP is also a source of CN^- anions. Infusion at too elevated rates (or at too high concentration) leads to cyanide toxicity[4,5]. A way to control release over time of any drug in the blood stream is encapsulation of the Active Pharmaceutical Ingredient (API) in a host structure[6]. In the field of biomedicine, silica matrices are interesting in this way[7–9] as they offer a good biocompatibility[10,11]. Nevertheless, confinement induces changes upon the environment of the API, which may have an impact on molecular properties[12]. These have to be perfectly well-defined to ensure possible medical applications for the drug delivery system with its encapsulated compound. Additionally, designing the porous structure of the matrix structure allows release rates of APIs to be adjusted[13], as host-guest interactions can be modulated[14]. It is therefore very important to provide insight on the main three aspects that rule the properties of the vectorized API, namely: structure, dynamics and host-guest interactions inside the confined environment.

To this intent, selectively labeled $Na_2[Fe(^{13}CN_5)^{15}NO]$, that is to say S[NP], is confined within an amorphous porous silica matrix, with pores of 1-2 nm in diameter. The result is a host-guest structure such that a single SNP complex is held within a pore (Figure 1). This structure has previously been characterized[15] thanks to complementary pair distribution function analysis (PDF) and solid state NMR (SS-NMR) analysis. The PDF analysis provided direct structural evidence on the local cation and anion arrangement of the SNP. It was suggested that sodium ions have a preferential positioning in the equatorial plane of the nitroprusside anion, in the continuity of the Fe-C≡N bonds, at 5.5 Å distance of the complex center and that the complex remains therefore associated. This optimum configuration was established by minimizing the difference between calculated pair distribution functions for

different placement of the two sodium ions and experimental data. SS-NMR added a supplementary dynamic dimension to the static structural characterization: within this confined environment, this technique suggested a dissolved state for SNP. Indeed, even while working with a powder, ^{13}C spectra displayed no spinning side bands, indicating isotropic motion of the complex. We therefore decided to perform in the current study a quantitative analysis of the dynamical properties of the guest molecules, in order to gather more information about how these two models can coexist. The objective here, is to understand how both ions of the SNP complex can be subjugated to sub-microsecond isotropic motion, while retaining a complex associated structure.

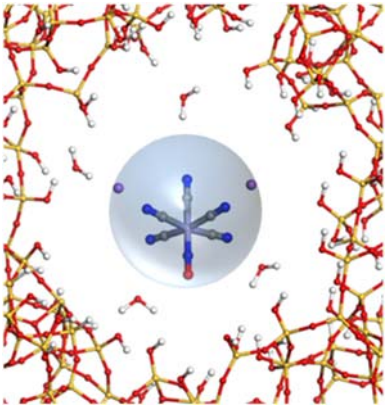

Figure 1: Illustration of one associated $Na_2[Fe(CN_5)NO]$ (SNP) complex confined inside the 1-2nm diameter silica matrix pores. The complex's structural model was established with the Reverse Monte-Carlo method and total scattering data as described in ref [15]. A few water molecules have been arbitrarily added to the figure for a more realistic view. Hydrogen atoms are labeled in white, Silicon in yellow, Oxygen in red, Nitrogen in Blue, Carbon in Grey, Sodium in purple, and the Iron atom is located at the center of the complex.

In addition to providing chemically resolved information, NMR is a suitable analysis technique to extract information about molecular dynamics[16–19]. First, by considering different nuclei (^{13}C, ^{23}Na, ^{1}H and ^{29}Si), it is easy to select the different species present in our system: NP anions, sodium counter-ions, water / silanols and the matrix respectively. In order to have

reliable NMR measurements for evaluating the dynamics of these different species, SNP molecules were here selectively labeled for a better sensitivity. Secondly, from the dependence of longitudinal relaxation times (T_1) of ^{13}C and ^{23}Na on temperature variations, motional activation energies can henceforth be obtained[20]. By comparing their respective values, correlation in the molecular tumbling of the different ionic species may step into the light. In this work, the effect of solvating water molecules inside the pores of the matrix will also be discussed, the storage relative humidity (RH) becoming a new parameter in the structural description of our vectorized API. Indeed, water content inside the pores turns out to be very impactful on the structure of the confined drug and host-guest interactions. In particular, for the driest sample condition, we are able to find hints toward why bulk-like crystallization of SNP has been observed inside pores with diameters as small as 6 nm[21].

2) Experimental section

a) Materials

For the synthesis of the porous silica matrix we used tetramethoxysilane (TMOS, Fluka) and methanol (VWR). Synthesis of isotopically labeled $Na_2[Fe(^{13}CN_5)^{15}NO]$ was performed from $Na[^{13}CN]$ and $Na[^{15}NO_2]$ (Eurisotop).

b) Sample preparation

Synthesis of isotopically labeled $Na_2[Fe(^{13}CN_5)^{15}NO]$ was performed as previously reported by Hyde and co-workers[22,23]. We used the porous silica matrices synthesized during our previous study[15] and slowly performed impregnation with $Na_2[Fe(^{13}CN_5)^{15}NO]$ during 48h to avoid any cracking. After quick water washing of the impregnated matrix in order to avoid any SNP crystallization outside of the pores, the material was kept at 323K for a week in an oven. Subsequently, the matrices were ground to powder with mortar and pestle and filled inside 4mm MAS NMR rotors. To allow for in-situ sample temperature measurements, the

rotors were filled with about 40wt% of KBr, 40wt% of SNP@SiO_2 and separated by 20%wt Teflon tape. Open rotors were kept at least 48h before any kind of NMR analysis in a hermetic container with saturated solutions of LiBr, $CaCl_2$ and KCl salts stabilizing the atmosphere at 6% (sample A), 29% (sample B) and 85% (sample C) relative humidity respectively[24,25] (at 298K). Sample A' refers to sample A after it has been extensively dried for 48h, at 323 K, with a turbo-molecular vacuum pump at 10^{-4} mbar.

c) NMR Experiments

All experiments are conducted on a high-field Bruker NMR Avance III spectrometer operating at 14T (^{1}H NMR frequency of 600 MHz) with a Bruker 4mm MAS triple-resonance probe.

For ^{13}C direct excitation MAS experiments, the rf-field strength applied for the 90° pulse was set to 50 kHz, for a length of 5µs. During acquisition, SPINAL-64 heteronuclear decoupling[26] was applied at an rf-field strength of 31.25 kHz with a pulse length of 8 µs. For the hydrated SNP@SiO_2 samples (A, B and C) the interscan delay was set to 3 s and 128 scans were accumulated for a total experimental time of about 7min. For the dried SNP@SiO_2 sample (A') the interscan delay was set to 50s and 800 scans were accumulated for a total experimental time of about 11h. R_1 relaxation experiments where performed with a saturation-recovery pulse sequence at a MAS spinning speed of 5 kHz with 11 different time intervals chosen to best describe the relaxation recovery curve. For ^{1}H-^{13}C CPMAS and CP-HETCOR excitation experiments, Hartmann-Hahn conditions[27] matched a ^{13}C field of 35.8 kHz with a ^{1}H field of 50 kHz (90-100 ramp) during a 2.35 ms contact time. For ^{1}H-^{13}C CPMAS experiments, the interscan delay was set to 3 s and 7168 scans were accumulated for a total experimental time of 6 h. The 2D ^{1}H/^{13}C CP-HETCOR spectrum[28] was recorded with 368

scans and 3s recycle delay, while MAS was set at 12.5 kHz. Indirect dimension was sampled in 64 points with a dwell time of 80µs for a total experimental time of about 20 h.

For ^{23}Na MAS experiments the rf-field strength applied for the 90° pulse was set to 55.5 kHz, for a length of 4.5µs. As for ^{13}C experiments, SPINAL-64 heteronuclear decoupling was also performed. The interscan delay was set to 2 s and 64 scans were accumulated for a total experimental time of about 2min. As for ^{13}C experiments R_1 relaxation experiments where performed with a saturation-recovery pulse sequence.

For the ^{1}H-^{29}Si{^{13}C} REDOR experiment, a sequence with dephasing π pulses (at 50 kHz) placed each half-rotor period on the non-observed channel (^{13}C) and a unique refocusing π pulse (at 50 kHz) in the middle of the echo sequence on the observed nucleus (^{29}Si) was used while MAS was set to 12.5 kHz. REDOR π pulses employed xy8 phase cycling for the refocusing and recoupling pulses[29]. Data acquisition employed an alternating block scheme, collecting a single S_0 transient with recoupling pulses turned off, followed by S_R transient collection with recoupling pulses turned on. Spectra are recorded with 8192 scans and 3s recycle delay for a total experimental time of about 13.5 h. REDOR data were collected using a CP-MAS excitation scheme where ^{1}H / ^{29}Si Hartmann-Hahn conditions matched a ^{1}H field of 30.7 kHz (90-100 ramp) with a ^{29}Si field of 33.2 kHz during a 4 ms contact time.

Real sample temperature (±0,1 K) was monitored in-situ before each experiment by measuring the ^{79}Br chemical shift of the KBr included in the MAS rotor[30]. For temperatures to reach equilibrium, we waited 10 minutes before any NMR measurement. Cooling of the MAS sample was performed using N_2 gas pre-cooled inside a home-made temperature exchange Dewar.

The Dmfit program[31] was used for spectral deconvolution and to fit ^{13}C chemical shift anisotropy based on MAS sideband patterns. Mathematica 10.3 software was used to fit the

saturation-recovery T_1 relaxation curves, the R_1 as a function of 1/T plots, and to perform the corresponding statistical analysis.

The ^{1}H, ^{13}C and ^{29}Si chemical shifts are reported relative to TMS.

3) Results and Discussion

a) Hydrated samples

To assess the effect of solvating water molecules on the confined guest's dynamics, we performed our measurements on samples of SNP@SiO_2 stored at different Relative Humidity (RH) levels. Samples of SNP@SiO_2, as used in our previous study[15], and stored at 29% (sample B) and 85% (sample C) relative humidity are first considered. Figure 2 shows a comparison of ^{13}C MAS NMR spectra for samples: A' (vacuum dried), A (stored at 6% RH), B (stored at 29% RH) and C (stored at 85% RH). For comparison, the spectrum of crystalline SNP is also plotted along with the others. It appears that for static SNP in its crystalline form, the ^{13}C MAS spectrum exhibits intense chemical shift anisotropy (CSA) spinning sidebands originating from the anisotropy of the electron distribution in the Fe-C≡N bonds. Since the MAS sidebands origin is intramolecular, their reduction in a spectrum is necessarily due to motional averaging. Comparison of the spectra plotted in Figure 2 shows that strong motional CSA averaging occurs for hydrated samples B and C. Indeed, as room temperature ^{13}C MAS spectra of these samples consist mainly of a sharp line instead of presenting a rigid powder pattern, the nitroprusside [NP] anions behave as in a liquid-like state inside the pores of the silica matrix. Conversely, [NP] inside samples A and A' exhibits significant MAS sidebands which means that the ions are not subject to isotropic motion on the sub millisecond timescale. The results on these dry samples will therefore be discussed in the next section.

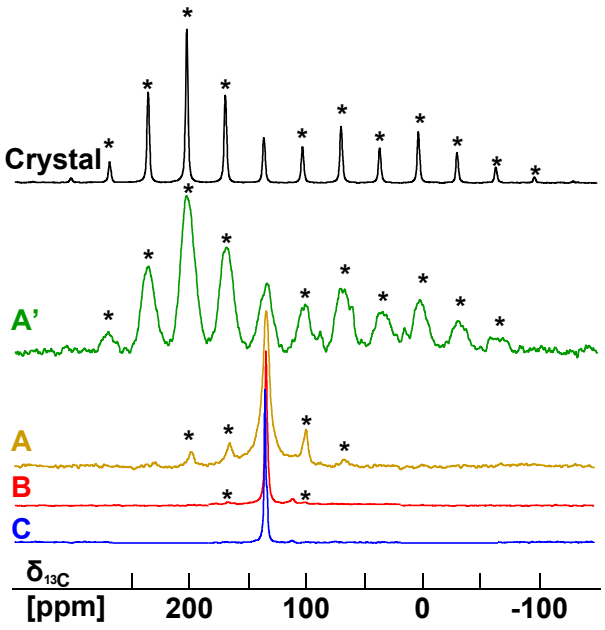

Figure 2: ^{13}C spectrum of crystalline SNP and ^{13}C spectra of confined SNP (samples A', A, B and C) at 5 kHz MAS. The signal at 111ppm originates from Teflon tape spacers inside the MAS rotor. 200 Hz of line broadening is applied to all spectra.

In order to evaluate the molecular dynamics observed inside the pores, T_1 relaxation times are measured at various temperatures for ^{13}C, ^{23}Na and ^{1}H spins, to focus respectively on NP anions, sodium counterions and water molecules. Strong anisotropy of the Fe-C≡N bonds implies that ^{13}C (I=1/2) T_1 relaxation is mainly driven by its CSA, allowing mono-exponential fit of the experimental data. For each considered sample and temperature, ^{23}Na (I=3/2) 1D spectra consist of one sharp peak. Therefore, quadrupolar interaction is shown to be averaged by fast dynamics, thus also allowing a mono-exponential fit for T_1[32] (Figure S1 in SI).

In Figure 3 we plot $R_1=1/T_1$ on a logarithmic scale against the inverse of temperature. In the higher temperature domain (T > 278 K and T > 246 K respectively for samples B and C), we notice a linear correlation between $\ln(R_1)$ and 1/T. Fast motion limit can thus be assumed and justifies the proportionality between R_1 and τ_c ($\omega_0*\tau_c<<1$ with $\omega_0/2\pi$ the resonance

frequency and τ_c the correlation time describing the motion) [33]. Using Arrhenius' law[34,35] the motional activation energies (Ea) can then be determined from the slope of the curve (Ea/R, with R=8.314 J.mol^{-1}.K^{-1}).

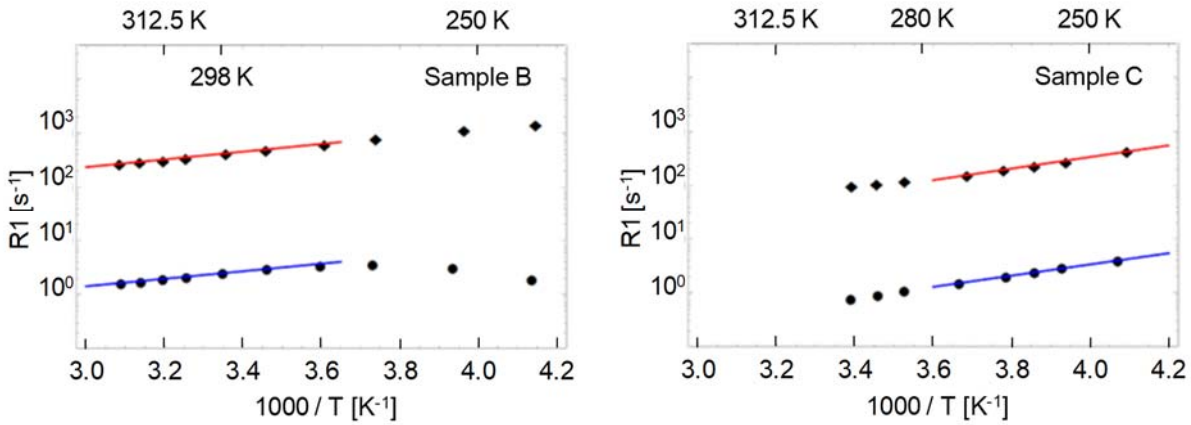

Figure 3: Longitudinal relaxation rates R_1 in seconds^{-1} plotted on a logarithmic scale as a function of the inverse of the temperature for sample B, RH=29% (left) and C, RH=85% (right). ^{13}C data are plotted with circles, and ^{23}Na with diamonds. Solid lines represent linear regressions taken to extract associated activation energies.

For each hydration level, we find a common temperature interval for ^{13}C (probing NP dynamics), ^{23}Na (counterion) and ^{1}H (water) nuclei yielding linear evolution of data with a good correlation coefficient R^2>0.99. The corresponding activation energies, which are in the expected range for small confined molecules[36], are summarized in Table 1. For 29% relative humidity storage (sample B), the temperature interval, within which the equality $Ea^{NP}=Ea^{Na}$ is verified, includes 298K, that is to say the experimental condition for which our structural model was previously established by PDF analysis. The equal values of activation energy found for both ions of the SNP complex are strong arguments in favor of asserting a correlated movement of the ions. This conclusion is reinforced by the fact that water presents

far lower activation energy, which means that its movement is independent to the one of the SNP ion pair. Analysis of the hydrated sample B shows that our prior structural models provided by PDF and NMR techniques are therefore converging toward a coherent and unique result: inside the 1-2nm pores of the silica matrix, on the [278 K ; 324 K] temperature interval, the fully associated SNP complex follows an isotropic motion with a positioning of the Na cations in the nitroprusside equatorial plane. It is therefore not in a fully liquid-like state.

Table 1: Motional activation energies of the different confined species in kJ.mol-1, with errors established while allowing a 95% confidence interval on T_1 fits.

Sample	NP	Na	Water	Temperature interval(in K) from which Ea is calculated
B	13.3 ±0.9	13.7 ±1.4	2.5 ±0.1	[278 ; 324]
C	19.8 ±0.2	20.4 ±1.6	5.55 ±0.05	[246 ; 271]

The equality $Ea^{NP}=Ea^{Na}$ is also verified for the most hydrated sample C (89% RH) within [246 K ; 271 K]. Above 271K, the equality does not hold anymore. Indeed, to the contrary of ^{13}C relaxation data, when ^{23}Na experimental data for temperatures above 271K are included in the analysis, the linear correlation coefficient starts to degrade, pointing towards a possible reduction of the motional activation energy. This temperature may thus mark a threshold above which dissociation of the SNP ion pair occurs in the more hydrated sample.

b) Dried samples

Figure 4 presents the plot of ^{13}C and ^{23}Na R_1 relaxation against temperature for a sample of SNP@SiO_2 stored at 6% relative humidity (sample A). It shows that no single linear evolution with a satisfactory R^2 (>0.99) can be found within our measurement range and indicates more complex dynamics than when dealing with hydrated samples.

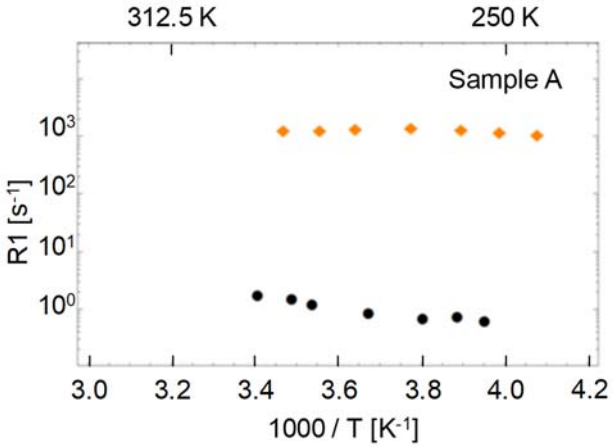

Figure 4: ^{13}C (circles) and ^{23}Na (diamonds) longitudinal relaxation rates R_1 in seconds^{-1} plotted as a function of the inverse of the temperature for sample A, RH=6%

Comparison of 1D MAS spectra provides more insight into the behavior of SNP ions in these conditions. To the contrary of samples B and C, the ^{13}C spectrum of sample A reflects the loss of the isotropic motion as rotational sidebands arise (Figure 2b). The intensity of MAS sidebands on ^{13}C spectra allow an evaluation of the chemical shift anisotropy (CSA) and fitting those intensities provides an estimate of how much the mobility is reduced at room temperature. Results are presented in Table 2. Since its ^{13}C CSA is essentially intramolecular, crystalline SNP is used as a static reference ($\Delta\sigma$= -212 ppm in the Haeberlen convention[37]). ^{13}C MAS spectrum of sample A exhibits a residual CSA of $\Delta\sigma$= 56 ppm, which may be

caused by intermediate averaging of the CSA by anisotropic motion or exchange (between free and adsorbed NP) below the microsecond time scale.

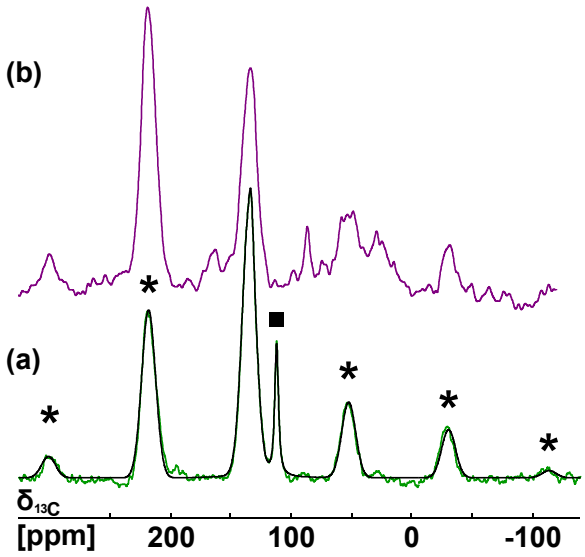

Figure 5: Comparison of sample A' ^{13}C MAS spectra (12.5 kHz) obtained by direct acquisition with its deconvolution (a) and by CP-MAS (b). MAS spinning sidebands are marked by asterisks and background signal from Teflon tape spacers by a square.

Table 2: Fitted Chemical Shift Anisotropy using Dmfit program[31], Δσ in ppm, according to Haeberlen's convention. In each case, the fitted asymmetry parameter η is equal to 0.

	Crystal	A'	A	B	C
Δσ [ppm]	-212	-207	56	56	-
Fraction of immobilized SNP	-	86 %	63 %	11 %	0 %

To better understand this behavior, we further lower the water content inside the pores. To that effect, sample A was dried for 48 hours at 50°C under a high vacuum (10^{-4} mbar) and is now referred to as sample A'. As seen on Figure 5a, efficient drying has direct impact on the ^{13}C spectrum, revealing a major component with a CSA value of about $\Delta\sigma$= -207ppm, comparable to the bulk crystal value ($\Delta\sigma$= -212 ppm). This result shows that removing water molecules inside the silica matrix decreases nitroprusside (NP) anion mobility down to the static value. For direct ^{13}C excitation (Figure 5a), two components are required to have a good fit agreement on the intensity of the central line at 133.2 ppm, therefore showing the coexistence of two NP populations. The predominant one corresponds to immobilized NP, whereas the second one exhibits a fully isotropic signal and is therefore assigned to free mobile NP. Allowing sufficient recovery time (t_{rec}=50s), every NP ion contributes to the spectrum and the ratio of the integrals yields that around 86% of NP is in the completely static state. This procedure has also been applied to sample A and B, where the more rigid population drops down to 63% and 11% respectively and displays a residual CSA of $\Delta\sigma$= 56ppm (Table 2). Depending on sample hydration, we can therefore identify three distinct NP populations undergoing different dynamics. In the driest sample (A'), NP is mostly fully immobilized ($\Delta\sigma$= -207ppm). In the presence of water molecules (samples A and B), a less mobile part of the NP is not completely static, as evidenced by the reduced CSA ($\Delta\sigma$= 56ppm). The third population is present in all samples and consists of NP that undergoes rapid isotropic reorientation completely averaging out the CSA. Restricted motion NP in dry samples is indicative of an interaction between NP and the inner surface of the silica pores. This presence of two "bound" and one "free" populations is very similar to what has been observed for amino acids in SBA-15 and MCM-41 type mesoporous materials[38–41]. Indeed, distinct dynamic states of the adsorbed biomolecules were detected and the authors identified

one tightly bound, one loosely bound, and one free amino acid population depending on hydration level and temperature.

To focus on the surface bound NP population, acquisition of ^{13}C spectra was also performed with $^{1}H/^{13}C$ cross polarization (CP) (Figure 5b). Evidence of a host/guest interaction lies already in the possibility to actually perform $^{1}H/^{13}C$ cross polarization in sample A', since the only source of protons originates from the surface silanol groups (and eventual residual surface bound water molecules). Figure 5b shows the ^{13}C CP-MAS spectrum, where only the static population can be observed. In order to verify our interpretation, a 2D $^{1}H/^{13}C$ CP-HETCOR spectrum has also been acquired[42]. From the chemical shifts in the ^{1}H dimension, one may determine from which kind of proton (isolated silanol, free water, hydrogen-bonded proton, …) the magnetization is transferred to ^{13}C during CP[43,44].

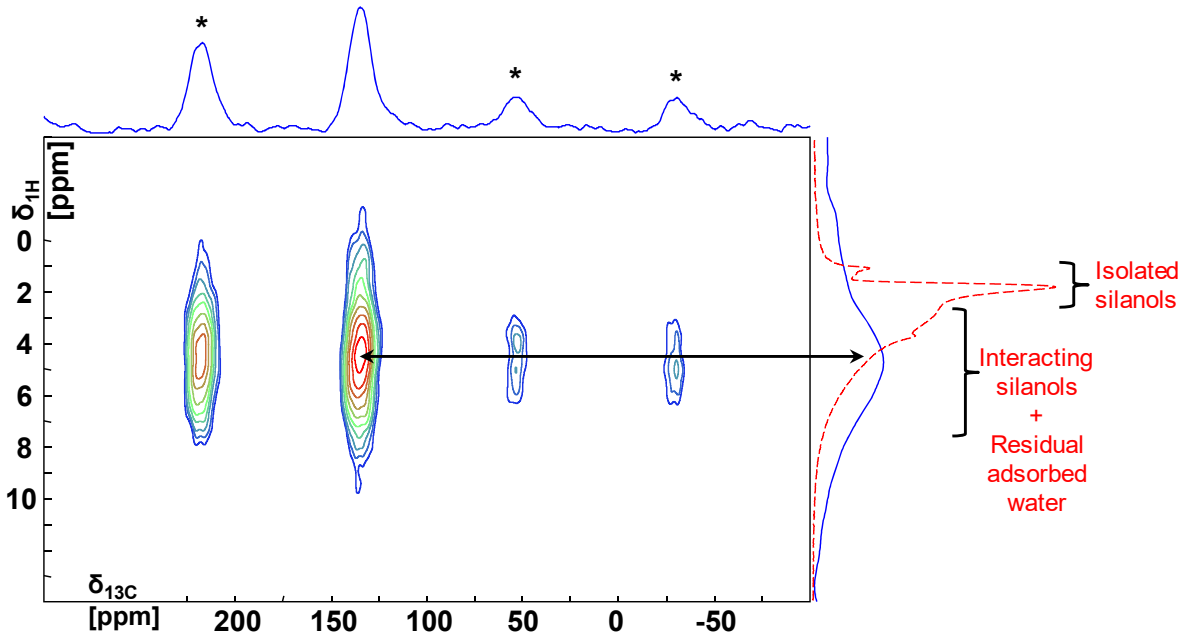

Figure 6: ^{1}H / ^{13}C heteronuclear CP correlation experiment with projections (continuous line) and comparison with 1D proton spectrum (dashed line).

Figure 6 shows that ^{13}C sites from NP correlate to a broad proton signal centered at 4.3 ppm. Such a chemical shift typically corresponds to protons subject to hydrogen bonding at the pore surface of amorphous silica matrices. This chemical shift is usually assigned to

vicinal surface silanol groups interacting together, or to adsorbed water interacting with surface silanols, or to silanol protons in exchange with free water[44]. Since sample A' has been extensively dried, we can rule out presence of free water. This is confirmed by the absence of a corresponding narrow peak around 5ppm on the 1D ^{1}H spectrum (right side of figure 6). Therefore we can assign this site to ^{1}H possibly involved in three different types of H-bonding: vicinal silanol bridge; silanol/"bound water" interaction; and silanol/NP with N-H hydrogen bonding.

To further investigate the NP/silanol interaction we performed a ^{1}H-$^{29}Si\{^{13}C\}$ REDOR dephasing experiment[29] that allows the detection of heteronuclear dipolar interactions by comparing a reference ^{29}Si spectrum (S0) to a so called "dipolar dephased" spectrum (Sr), where rotor-synchronized π-pulses on the ^{13}C channel reintroduce MAS averaged heteronuclear dipolar couplings. For specific conditions, dephasing time evolution of the Sr/S0 intensity ratio may even allow quantitative distance measurements[40,45]. If an isolated pair of $^{13}C/^{29}Si$ spins is considered, the Sr/S0=f(t) dephasing curve should fit a damped Bessel function. Thus, it should present an initial decrease, followed by a modulation around a plateau centered on 0; the initial steep and the oscillation frequency reflecting the ^{13}C-^{29}Si spin pair distance through its dipolar coupling. However, because of the presence of multiple ^{29}Si-^{13}C couplings in our uniformly ^{13}C-labelled molecular system and the relatively long ^{29}Si-^{13}C distances involved, the acquired Sr/S0 curve (Figure S2) does not exhibit these characteristic dipolar oscillations. Therefore, our dataset is not sufficient to allow the quantitative determination of ^{13}C-^{29}Si distances, or second moment[46], as published in other studies[39–41], since in the host matrix all detected ^{29}Si spins are not in the vicinity of NP ions and we thus cannot normalize the curve to the maximum relative attenuation.

Nevertheless, important qualitative information can be retrieved from Figure 7, where the difference signal between S0 and Sr for 50 ms dephasing time is presented. This significant

dephasing provides clear evidence of a dipolar interaction between NP ^{13}C and silanol ^{29}Si. The ability to still observe this $^{13}C/^{29}Si$ interaction does not leave any space for water molecules intercalated between NP anions and the surface silanols, and therefore gives an additional confirmation that the observed correlation on the HETCOR spectrum is effectively directly between NP and silanol ^{1}H.

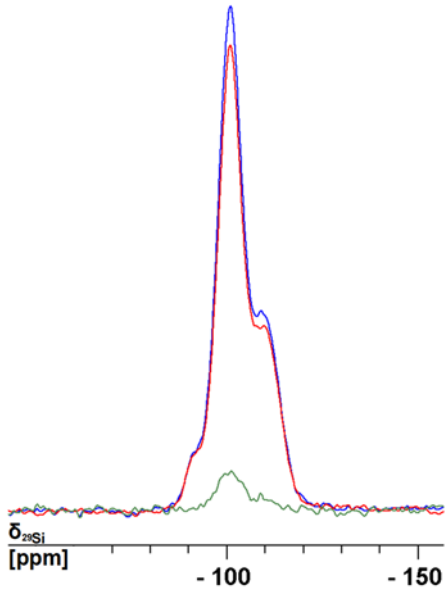

Figure 7: Reference and dephased ^{1}H-$^{29}Si\{^{13}C\}$ REDOR spectra (50ms echo): Reference S0 in blue, dephased Sr in red and difference spectra in green. Sr/S0≈8,2%. We verified that this dephasing does not originate from electronic instabilities by performing the same experiment on an empty Sol-Gel SiO_2 matrix (Figure S3).

Consequently, the correlation observed on Figure 6 with protons resonating at 4.3 ppm could well involve a silanol hydrogen-bonded to a NP cyanide nitrogen atom. Indeed, if the NO part was committed in the hydrogen bond, Si-C distances would be too large to allow REDOR dephasing. However, the assumption of such a strong hydrogen bond would imply a major difference in the expected chemical shift, as several studies report values between 7 and 10 ppm for such protons[47–49]. An upfield shift to 4.3ppm could nevertheless result from the

weakening of the hydrogen bond due to several nitrogen atoms of the same NP ion interacting simultaneously with the surface and possibly exchanging their interaction site on a sub-ms timescale. Finally, a remaining option for the attribution of the 4.3ppm ^{1}H correlation corresponds to spatially close pairs of silanols already involved in a hydrogen bond with one another. However, this would not explain the origin of the NP-Si interaction. Further investigations will have to be performed in order to characterize this interaction. Future work dedicated to the characterization of the host/guest interaction should involve additional ^{1}H-$^{29}Si\{^{15}N\}$ and ^{1}H-$^{29}Si\{^{23}Na\}$ REDOR experiments along with molecular dynamic simulations to derive structural models for the Nitroprusside and Sodium guests interacting with the matrix's surface.

Furthermore, unraveling these host/guest interactions, masked in presence of competing water molecules, gives us a hint towards why bulk-like crystallization of SNP could be observed inside pores with diameters as small as 6 nm[21]. Such crystallization may indeed seem surprising as pore diameters are smaller than ten times the size of an SNP complex (about 0.8 nm), since for such small pore sizes usually no crystallization occurs [50–52]. In that respect, NP adsorption on the pore surface reduces its mobility, which induces favorable conditions for nucleation to happen. This interaction may thus be the key to understanding this system's confined crystallization process.

4) Conclusions

When dealing with hydrated samples, temperature evolutions of ^{13}C and ^{23}Na longitudinal T_1 relaxation times allowed us to quantify motional activation energies of guest species (NitroPrusside and its Sodium counterions) inside 1-2 nm pores of a silica matrix. Their equal values show that both elements of a single Sodium Nitroprusside (SNP) complex are animated with an isotropic but correlated movement, on specific temperature intervals. As a result, for these conditions SNP is indeed in a liquid-like state; however ions are not

dissociated. This result confirms the conclusions from our previous study by bringing coherence between the proposed structural model and the observed dynamical properties of the complex[15]. We also showed the limits of these conclusions on dry samples, since a presence of residual ^{13}C CSA indicates restricted motion and ^{1}H-^{13}C polarization transfer demonstrates the existence of populations of adsorbed NP. In particular, by comparing ^{13}C spectra obtained through direct excitation and cross polarization we could detect and quantify the presence of two types of bound populations depending on the extent of residual water in the matrix. Removing all free water molecules also enabled us to perform $^{1}H/^{13}C$ CP HETCOR and complementary ^{1}H-$^{29}Si\{^{13}C\}$ REDOR experiments. Even though these experiments were not enough to precisely characterize the host/guest interaction, they nonetheless reveal an interaction between NP anions and surface silanols of the matrix that was otherwise masked by water molecules. We therefore speculate that this interaction is probably a key to understand why we previously observed an unusually high crystallization propensity in silica matrices with 6 nm pores. The results found here show the existence of an affinity between silanols and NP ions which would point to a nucleation growth process for the crystallization mechanism in the confined environment.

5) Supporting Information

The following PDF file is available free of charge. S1: ^{1}H, ^{13}C and ^{23}Na saturation-recovery data for samples A (at 288 K), B (298 K) and C (254 K). S2: REDOR dephasing curve. S3: ^{1}H-$^{29}Si\{^{13}C\}$ REDOR on an empty silica matrix as a carbon-free reference.

6) Acknowledgements

The work was partially financed by Lorraine Université d'excellence (award No. ANR-15-IDEX-04-LUE). We acknowledge the help of Peter Klüfers and Xaver Kästele for the synthesis of isotopically-labeled samples.

7) References

(1) Bates, J. N.; Baker, M. T.; Guerra Jr., R.; Harrison, D. G. Nitric Oxide Generation from Nitroprusside by Vascular Tissue: Evidence That Reduction of the Nitroprusside Anion and Cyanide Loss Are Required. *Biochem. Pharmacol.* **1991**, *42*, *Supplement 1*, S157–S165.

(2) Wang, Z.; Wen, F.; Zhang, R.; Zhang, Q. Modulated Nitric Oxide Delivery in Three-Dimensional Biomaterials for Vascular Functionality. *MRS Commun.* **2017**, *7* (03), 348–360.

(3) Belani, K.; Hottinger, D.; Kozhimannil, T.; Prielipp, R.; Beebe, D. Sodium Nitroprusside in 2014: A Clinical Concepts Review. *J. Anaesthesiol. Clin. Pharmacol.* **2014**, *30* (4), 462.

(4) Friederich, J. A.; Butterworth, J. F. Sodium Nitroprusside: Twenty Years and Counting. *ANESTH ANALG* **1995**, 11.

(5) Vesey, C. J.; Cole, P. V.; Simpson, P. J. Cyanide and Thiocyanate Concentrations Following Sodium Nitroprusside Infusion in Man. *Br. J. Anaesth.* **1976**, *48* (7), 651–660.

(6) Kim, S.; Stébé, M.-J.; Blin, J.-L.; Pasc, A. PH-Controlled Delivery of Curcumin from a Compartmentalized Solid Lipid Nanoparticle@mesostructured Silica Matrix. *J Mater Chem B* **2014**, *2* (45), 7910–7917.

(7) Bitar, A.; Ahmad, N. M.; Fessi, H.; Elaissari, A. Silica-Based Nanoparticles for Biomedical Applications. *Drug Discov. Today* **2012**, *17* (19–20), 1147–1154.

(8) Wang, Y.; Zhao, Q.; Han, N.; Bai, L.; Li, J.; Liu, J.; Che, E.; Hu, L.; Zhang, Q.; Jiang, T.; et al. Mesoporous Silica Nanoparticles in Drug Delivery and Biomedical Applications. *Nanomedicine Nanotechnol. Biol. Med.* **2015**, *11* (2), 313–327.

(9) Bharti, C.; Nagaich, U.; Pal, A. K.; Gulati, N. Mesoporous Silica Nanoparticles in Target Drug Delivery System: A Review. *Int. J. Pharm. Investig.* **2015**, *5* (3), 124–133.

(10) Tang, F.; Li, L.; Chen, D. Mesoporous Silica Nanoparticles: Synthesis, Biocompatibility and Drug Delivery. *Adv. Mater.* **2012**, *24* (12), 1504–1534.

(11) He, Q.; Shi, J. Mesoporous Silica Nanoparticle Based Nano Drug Delivery Systems: Synthesis, Controlled Drug Release and Delivery, Pharmacokinetics and Biocompatibility. *J. Mater. Chem.* **2011**, *21* (16), 5845.

(12) Komori, Y.; Hayashi, S. Dynamics of P-Nitroaniline Molecules in FSM-Type Mesoporous Silicas Studied by Solid-State NMR. *Microporous Mesoporous Mater.* **2004**, *68* (1–3), 111–118.

(13) Barbé, C.; Bartlett, J.; Kong, L.; Finnie, K.; Lin, H. Q.; Larkin, M.; Calleja, S.; Bush, A.; Calleja, G. Silica Particles: A Novel Drug-Delivery System. *Adv. Mater.* **2004**, *16* (21), 1959–1966.

(14) Vallet-Regí, M.; Balas, F.; Arcos, D. Mesoporous Materials for Drug Delivery. *Angew. Chem. Int. Ed.* **2007**, *46* (40), 7548–7558.

(15) Hsieh, K.-Y.; Bendeif, E.-E.; Gansmuller, A.; Pillet, S.; Woike, T.; Schaniel, D. Structure and Dynamics of Guest Molecules Confined in a Mesoporous Silica Matrix: Complementary NMR and PDF Characterisation. *RSC Adv.* **2013**, *3* (48), 26132.

(16) Canet, D. Introduction: General Theory of Nuclear Relaxation. In *Advances in Inorganic Chemistry*; Elsevier, 2005; Vol. 57, pp 3–40.

(17) Steiner, E.; Bouguet-Bonnet, S.; Blin, J.-L.; Canet, D. Water Behavior in Mesoporous Materials As Studied by NMR Relaxometry. *J. Phys. Chem. A* **2011**, *115* (35), 9941–9946.

(18) Meier, B. H.; Graf, F.; Ernst, R. R. Structure and Dynamics of Intramolecular Hydrogen Bonds in Carboxylic Acid Dimers: A Solid State NMR Study. *J. Chem. Phys.* **1982**, *76* (2), 767–774.
(19) Gul-E-Noor, F.; Michel, D.; Krautscheid, H.; Haase, J.; Bertmer, M. Investigation of the Spin-Lattice Relaxation of ^{13}CO and $^{13}CO_2$ Adsorbed in the Metal-Organic Frameworks Cu_3 $(Btc)_2$ and Cu_{3-x} Zn_x $(Btc)_2$. *J. Chem. Phys.* **2013**, *139* (3), 034202.
(20) Tritt-Goc, J.; Pislewski, N. Proton NMR Relaxation Study of the Motion of Water Molecules in Hydrated Nitroprussides. *J. Phys. Chem. Solids* **1993**, *54* (1), 123–126.
(21) Bendeif, E.-E.; Gansmuller, A.; Hsieh, K.-Y.; Pillet, S.; Woike, T.; Zobel, M.; Neder, R. B.; Bouazaoui, M.; El Hamzaoui, H.; Schaniel, D. Structure Determination of Molecular Nanocomposites by Combining Pair Distribution Function Analysis and Solid-State NMR. *RSC Adv* **2015**, *5* (12), 8895–8902.
(22) Butler, A. R.; Glidewell, C.; Hyde, A. R.; McGinnis, J. Homonuclear Spin-Spin Coupling through Iron in Simple Inorganic Ions. *Polyhedron* **1984**, *3* (9–10), 1165–1167.
(23) Butler, A. R.; Glidewell, C.; Hyde, A. R.; McGinnis, J. Nitrogen-15 and Carbon-13 NMR Study of Roussin Salts and Esters and of Pentacyanoferrate Complexes. *Inorg. Chem.* **1985**, *24* (19), 2931–2934.
(24) Greenspan, L. Humidity Fixed-Points of Binary Saturated Aqueous-Solutions. *J. Res. Natl. Bur. Stand. Sect. -Phys. Chem.* **1977**, *81* (1), 89–96.
(25) Winston, P. W.; Bates, D. H. Saturated Solutions For the Control of Humidity in Biological Research. *Ecology* **1960**, *41* (1), 232–237.
(26) Fung, B. M.; Khitrin, A. K.; Ermolaev, K. An Improved Broadband Decoupling Sequence for Liquid Crystals and Solids. *J. Magn. Reson.* **2000**, *142* (1), 97–101.
(27) Hartmann, S. R.; Hahn, E. L. Nuclear Double Resonance in the Rotating Frame. *Phys. Rev.* **1962**, *128* (5), 2042–2053.
(28) Caravatti, P.; Bodenhausen, G.; Ernst, R. R. Heteronuclear Solid-State Correlation Spectroscopy. *Chem. Phys. Lett.* **1982**, *89* (5), 363–367.
(29) Gullion, T. Rotational-Echo, Double-Resonance NMR. In *Modern Magnetic Resonance*; Springer, 2008; pp 713–718.
(30) Thurber, K. R.; Tycko, R. Measurement of Sample Temperatures under Magic-Angle Spinning from the Chemical Shift and Spin-Lattice Relaxation Rate of 79Br in KBr Powder. *J. Magn. Reson.* **2009**, *196* (1), 84–87.
(31) Massiot, D.; Fayon, F.; Capron, M.; King, I.; Le Calvé, S.; Alonso, B.; Durand, J.-O.; Bujoli, B.; Gan, Z.; Hoatson, G. Modelling One- and Two-Dimensional Solid-State NMR Spectra: Modelling 1D and 2D Solid-State NMR Spectra. *Magn. Reson. Chem.* **2002**, *40* (1), 70–76.
(32) Woessner, D. E. NMR Relaxation of Spin-3/2 Nuclei: Effects of Structure, Order, and Dynamics in Aqueous Heterogeneous Systems. *Concepts Magn. Reson.* **2001**, *13* (5), 294–325.
(33) Kimmich, R. *NMR Tomography, Diffusometry, Relaxometry*; Springer Berlin: Berlin, 2013.
(34) Babanova, O. A.; Soloninin, A. V.; Skripov, A. V.; Ravnsbaek, D. B.; Jensen, T. R.; Filinchuk, Y. Reorientational Motion in Alkali-Metal Borohydrides: NMR Data for RbBH4 and CsBH4 and Systematics of the Activation Energy Variations. *J. Phys. Chem. C* **2011**, *115* (20), 10305–10309.
(35) Alam, T. M.; Dreyer, D. R.; Bielwaski, C. W.; Ruoff, R. S. Measuring Molecular Dynamics and Activation Energies for Quaternary Acyclic Ammonium and Cyclic Pyrrolidinium Ionic Liquids Using N-14 NMR Spectroscopy. *J. Phys. Chem. A* **2011**, *115* (17), 4307–4316.

(36) Lalowicz, Z. T.; Birczyński, A.; Krzyżak, A. Translational and Rotational Dynamics of Molecules Confined in Zeolite Nanocages by Means of Deuteron NMR. *J. Phys. Chem. C* **2017**, *121* (47), 26472–26482.
(37) Haeberlen, U. *Advances in Magnetic Resonance: Supplement*; Academic Pr, 1976.
(38) Jayanthi, S.; Kababya, S.; Schmidt, A.; Vega, S. Deuterium MAS NMR and Local Molecular Dynamic Model to Study Adsorption–Desorption Kinetics of a Dipeptide at the Inner Surfaces of SBA-15. *J. Phys. Chem. C* **2016**, *120* (5), 2797–2806.
(39) Ben Shir, I.; Kababya, S.; Schmidt, A. Molecular Details of Amorphous Silica Surfaces Determine Binding Specificity to Small Amino Acids. *J. Phys. Chem. C* **2014**, *118* (15), 7901–7909.
(40) Ben Shir, I.; Kababya, S.; Schmidt, A. Binding Specificity of Amino Acids to Amorphous Silica Surfaces: Solid-State NMR of Glycine on SBA-15. *J. Phys. Chem. C* **2012**, *116* (17), 9691–9702.
(41) Ben Shir, I.; Kababya, S.; Amitay-Rosen, T.; Balazs, Y. S.; Schmidt, A. Molecular Level Characterization of the Inorganic−Bioorganic Interface by Solid State NMR: Alanine on a Silica Surface, a Case Study. *J. Phys. Chem. B* **2010**, *114* (18), 5989–5996.
(42) Lesage, A.; Emsley, L. Through-Bond Heteronuclear Single-Quantum Correlation Spectroscopy in Solid-State NMR, and Comparison to Other Through-Bond and Through-Space Experiments. *J. Magn. Reson.* **2001**, *148* (2), 449–454.
(43) Grünberg, B.; Emmler, T.; Gedat, E.; Shenderovich, I.; Findenegg, G. H.; Limbach, H.-H.; Buntkowsky, G. Hydrogen Bonding of Water Confined in Mesoporous Silica MCM-41 and SBA-15 Studied by 1H Solid-State NMR. *Chem. – Eur. J.* **2004**, *10* (22), 5689–5696.
(44) Walia, J.; Crone, J.; Liang, J.; Niknam, M.; Lemaire, C.; Terry Thompson, R.; Peemoeller, H. Temperature and Hydration Dependence of Proton MAS NMR Spectra in MCM-41: Model Based on Motion Induced Chemical Shift Averaging. *Solid State Nucl. Magn. Reson.* **2013**, *49–50*, 26–32.
(45) Brückner, S. I.; Donets, S.; Dianat, A.; Bobeth, M.; Gutiérrez, R.; Cuniberti, G.; Brunner, E. Probing Silica–Biomolecule Interactions by Solid-State NMR and Molecular Dynamics Simulations. *Langmuir* **2016**, *32* (44), 11698–11705.
(46) Bertmer, M.; Eckert, H. Dephasing of Spin Echoes by Multiple Heteronuclear Dipolar Interactions in Rotational Echo Double Resonance NMR Experiments. *Solid State Nucl. Magn. Reson.* **1999**, *15* (3), 139–152.
(47) Shenderovich, I. G.; Buntkowsky, G.; Schreiber, A.; Gedat, E.; Sharif, S.; Albrecht, J.; Golubev, N. S.; Findenegg, G. H.; Limbach, H.-H. Pyridine- ^{15}N A Mobile NMR Sensor for Surface Acidity and Surface Defects of Mesoporous Silica. *J. Phys. Chem. B* **2003**, *107* (43), 11924–11939.
(48) Paul, G.; Musso, G. E.; Bottinelli, E.; Cossi, M.; Marchese, L.; Berlier, G. Investigating the Interaction of Water Vapour with Aminopropyl Groups on the Surface of Mesoporous Silica Nanoparticles. *ChemPhysChem* **2017**, *18* (7), 839–849.
(49) Guo, C.; Holland, G. P. Investigating Lysine Adsorption on Fumed Silica Nanoparticles. *J. Phys. Chem. C* **2014**, *118* (44), 25792–25801.
(50) Coasne, B.; Czwartos, J.; Sliwinska-Bartkowiak, M.; Gubbins, K. E. Freezing of Mixtures Confined in Silica Nanopores: Experiment and Molecular Simulation. *J. Chem. Phys.* **2010**, *133* (8), 084701.
(51) Sliwinska-Bartkowiak, M.; Dudziak, G.; Sikorski, R.; Gras, R.; Radhakrishnan, R.; Gubbins, K. E. Melting/Freezing Behavior of a Fluid Confined in Porous Glasses and MCM-41: Dielectric Spectroscopy and Molecular Simulation. *J. Chem. Phys.* **2001**, *114* (2), 950.

(52) Alba-Simionesco, C.; Dosseh, G.; Dumont, E.; Frick, B.; Geil, B.; Morineau, D.; Teboul, V.; Xia, Y. Confinement of Molecular Liquids: Consequences on Thermodynamic, Static and Dynamical Properties of Benzene and Toluene. *Eur. Phys. J. E - Soft Matter* **2003**, *12* (1), 19–28.

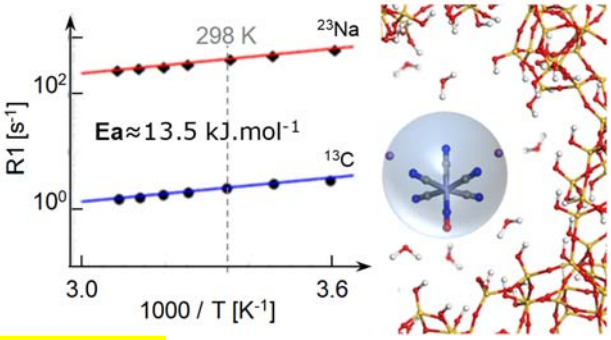

TOC Graphic